EUROPEAN ORGANIZATION FOR NUCLEAR RESEARCH

L3 Note 2762
July 1, 2002

Proton antiproton formation in Two-Photon Collisions at LEP

The L3 Collaboration

Abstract

The formation of a proton antiproton pair in two-photon collisions is studied with the L3 detector at LEP. The analysis is based on data collected at e^+e^- centre-of-mass energies from 183 GeV to 209 GeV, corresponding to an integrated luminosity of 667 pb^{-1}. The cross section as a function of the $\gamma\gamma$ centre-of-mass energy is measured and results are compared to those of other experiments and to predictions of the quark-diquark model.

Submitted to the 31st *International Conference on High Energy Physics*
Amsterdam, Netherlands, 24-31 July 2002.

1 Introduction

Electron-positron colliders are a suitable place for the study of two-photon interactions, via the process $e^+e^- \to e^+e^-\gamma^*\gamma^* \to e^+e^-X$, where γ^* denotes a virtual photon. The outgoing electron and positron carry almost the full beam energy and are usually undetected, due to their small transverse momenta. The final state X has, therefore, a low mass relative to the e^+e^- centre-of-mass energy, $\sqrt{s}$, and its transverse momentum is almost zero. The small photon virtuality allows the extraction of the cross section $\sigma(\gamma\gamma \to X)$ for real photon collisions, once the photon flux is calculated by QED [1].

In this note we present a study of the cross sections $\sigma(\gamma\gamma \to p\bar{p})$. The process $\gamma\gamma \to$ *baryon antibaryon* is sensitive to the quark structure of the baryon. Calculations of the cross section for this process were performed using the hard scattering approach [2]. Due to the failure of a three-quark calculation [3] to correctly predict the $\gamma\gamma \to p\bar{p}$ cross section in the GeV region [4], an alternative quark-diquark model was proposed [5]. This model includes non-perturbative effects through the use of diquarks, a qq bound state within the baryon [6]. In order to match the experimental acceptance with the range of the theoretical predictions, the data are analysed only in the region $|\cos\theta^*| < 0.6$, where θ^* is the polar angle of the proton in the two-photon centre-of-mass system.

We analyse a total integrated luminosity of 667 pb^{-1} collected with the L3 detector [7] at centre-of-mass energies from 183 GeV to 208 GeV. The analysis is based on the central tracking system and the high resolution BGO electromagnetic calorimeter. The events are selected by the track triggers [8].

The $p\bar{p}$ formation in two-photon collision was previously studied by the TASSO, JADE, TPC-2γ, ARGUS, CLEO and VENUS collaborations [4,9–13] at lower energies (Table 1). A preliminary analysis of OPAL data has been presented in Reference 14. Our results are compared to these experiments and to theoretical predictions of the quark-diquark model.

2 Monte Carlo simulation

Monte Carlo events for the $\gamma\gamma \to p\bar{p}$ reaction, as well as the $\gamma\gamma \to K^+K^-$ and $\gamma\gamma \to \pi^+\pi^-$ background processes, are generated [15] for each beam energy within the formalism of Reference 1. For each process a uniform spectrum as a function of the two-photon mass, $W_{\gamma\gamma}$, from threshold to 8 GeV is used. The two-body final states are generated isotropically in the centre-of-mass of the $\gamma\gamma$ system. The $e^+e^- \to e^+e^-\tau^+\tau^-$, $e^+e^- \to e^+e^-\mu^+\mu^-$ and $e^+e^- \to e^+e^-e^+e^-$ leptonic background are simulated with the DIAG36 [16] generator which calculate the full set of $O(\alpha^4)$ QED diagrams, including interference effects. The generated events are passed through the full L3 detector simulation using the GEANT [17] and GEISHA [18] programs and are reconstructed following the same procedure as for the data. Time dependent detector inefficiencies, as monitored during the data taking period, are taken into account.

3 Event Selection

Events are selected by requiring two well-reconstructed tracks of opposite charge. The tracks must lie in the central part of the detector, i.e. in the polar angle range $44° < \theta < 136°$. The track selection criteria are:

- a distance of closest approach to the interaction point in the transverse plane smaller than 3 mm,
- at least 30 hits out of a maximum of 62 in the tracking chamber,

- a transverse momentun greater than 500 MeV to ensure a high trigger efficiency,
- a corresponding signal in the electromagnetic calorimeter.

The identification of $\gamma\gamma \to p\bar{p}$ events is mainly based on the very characteristic signal of the antiproton annihilating in the electromagnetic calorimeter, as displayed in Figure 1, and on its dE/dx measurement in the central chamber. Three Neural Networks (NN) are used to separate antiprotons from e^-, μ^- and h^-, where $h^- = \pi^-$ and K^-. Each Neural Network consists of 5 input neuron, a single layer of 5 hidden neurons and one output neuron. The following measured quantities are associated with the 5 input neurons.

- The momentum of the antiproton.
- A probability based on the mean energy loss dE/dx measured in the tracker:

$$\frac{\mathrm{CL}(\bar{p})}{\mathrm{CL}(\bar{p}) + \mathrm{CL}(K^-) + \mathrm{CL}(\pi^-) + \mathrm{CL}(\mu^-) + \mathrm{CL}(e^-)}$$

  where CL(i) denotes the confidence level of being a particle of type i. This probability is close to 1 for well identified antiprotons and close to 0 for well identified K^-, π^-, μ^- or e^-.
- E_t/p_t, where E_t is the transverse energy measured in the electromagnetic calorimeter and p_t the transverse momentum measured in the tracker.
- The number of BGO crystals of the electromagnetic shower associated to the antiproton.
- The ratio between the energy deposited in the central crystal of the electromagnetic shower and the energy sum of the 9 crystals around the central crystal.

Each NN is trained with the corresponding sample from Monte Carlo simulations so that its output value, ζ, is close to 1 for antiprotons. To optimize the training process, the value of the different variables are normalized between 0 and 1. The performance of the NN is defined by its efficiency ε_i, rejection power r_i and purity $\mathcal{P}_i$:

$$\varepsilon_i = \frac{N_{pp}}{N_p} \qquad r_i = \frac{N_{ip}}{N_i} \qquad \mathcal{P}_i = \frac{N_{pp}}{N_{pp} + N_{ip}}$$

where N_{pp} is the number of antiprotons correctly identified as antiprotons, N_{ip} the number of i type particle wrongly identified as antiprotons, N_p the total number of antiprotons and and N_i the number of i type particles.

A particle is identified as an antiproton if the three NN outputs are greater than 0.9, i.e. $\zeta_e > 0.9$, $\zeta_\mu > 0.9$ and $\zeta_h > 0.9$, as shown if Figure 2. The performance of each NN for the corresponding identification criteria $\zeta > 0.9$ is presented in Table 2. Although the rejection power r_e and r_μ are larger than 99%, the electron and muon cross sections are more than two orders of magnitude greater than the $p\bar{p}$ production. The cuts on the e^- NN and h^- NN remove more than 99.9% of the remaining $e^+e^- \to e^+e^-\mu^+\mu^-$ background, whereas the $e^+e^- \to e^+e^-e^+e^-$ and $e^+e^- \to e^+e^-h^+h^-$ contamination still remain important. To reduce this background, the following cuts are applied to the proton candidate. The dE/dx measurement must be consistent with the proton hypothesis, requiring a CL > 0.05. This criteria removes background due to low momentum electrons, pions and kaons. The ratio between the electromagnetic transverse energy and the transverse momentum of the proton must also be less than 0.7. This requirement eliminates more than 97% of the remaining $e^+e^- \to e^+e^-e^+e^-$ background, as shown in Figure 2.

3.1 Exclusive $\gamma\gamma \to \mathrm{p\bar{p}}$ events

To select $\gamma\gamma \to \mathrm{p\bar{p}}$ exclusive events the following further cuts are applied

- Events with photon candidates are rejected. A photon candidate is defined as a shower in the electromagnetic calorimeter with at least two adjacent crystals and an energy greater than 100 MeV. Photon isolation criteria are also applied; there must be no charged tracks within 200 mrad around the photon direction and the cosine of the angle between the antiproton and the photon directions must be less than 0.8

- The square of the total transverse momentum of the proton antiproton pair $(\sum \vec{p_t})^2$ must be smaller than 0.1 GeV^2. This cut removes background events of the type $\mathrm{p\bar{p}X}$, where X represents one or more unobserved particles.

These cuts yield a total number of 604 selected events. The distribution of the effective mass of the $\mathrm{p\bar{p}}$ pair, $m_{\mathrm{p\bar{p}}}$, is presented in Figure 3.

The $\mathrm{e^+e^-} \to \mathrm{e^+e^-}K^+K^-$ and $\mathrm{e^+e^-} \to \mathrm{e^+e^-}\pi^+\pi^-$ background are estimated using the cross sections given in Reference 19 and processing the corresponding Monte Carlo events with the same analysis cuts. The background distributions as a function of $m_{\mathrm{p\bar{p}}}$ are presented in Figure 4. For each process, the background is found to be negligible in the region $m_{\mathrm{p\bar{p}}} < 2.5$ GeV and of the order of 5% above 2.5 GeV. An uncertainty of 50% on the $\mathrm{e^+e^-} \to \mathrm{e^+e^-}K^+K^-$ and $\mathrm{e^+e^-} \to \mathrm{e^+e^-}\pi^+\pi^-$ cross sections is included in the systematic uncertainties. The exclusive $\mathrm{e^+e^-} \to \mathrm{e^+e^-e^+e^-}$ and $\mathrm{e^+e^-} \to \mathrm{e^+e^-}\mu^+\mu^-$ background are found to be less than 0.2% and neglected.

The contamination of inclusive channels is estimated from the $(\sum \vec{p_t})^2$ distribution. The selected $\mathrm{p\bar{p}}$ sample is compared to the distribution expected from the $\mathrm{e^+e^-} \to \mathrm{e^+e^-p\bar{p}}$ Monte Carlo, as shown in Figure 5. The two distributions are normalized to the first three bins where the contamination is expected to be negligible. The difference between them is fitted with a straight line in the interval 0.2 GeV$^2 < (\sum \vec{p_t})^2 < 0.5$ GeV^2. The extrapolation to the region $(\sum \vec{p_t})^2 < 0.1$ GeV^2 gives a contamination of (1 ± 1)%, which we assume to be uniformly distributed in the $\mathrm{p\bar{p}}$ mass spectrum. Part of this background is due to $\mathrm{e^+e^-} \to \mathrm{e^+e^-}\tau^+\tau^-$ events. This contamination, estimated with the corresponding Monte Carlo, is less than 0.2%

The inclusive background, as well as the exclusive $\mathrm{e^+e^-} \to \mathrm{e^+e^-}K^+K^-$ and $\mathrm{e^+e^-} \to \mathrm{e^+e^-}\pi^+\pi^-$ background, are subtracted bin by bin for the cross section determination.

4 Results

The production cross sections $\sigma(\mathrm{e^+e^-} \to \mathrm{e^+e^-p\bar{p}})$ are measured as a function of the centre-of-mass energy for the following phase-space cuts: 2.1 GeV $< m_{\mathrm{p\bar{p}}} < 4.2$ GeV, $|\cos\theta^*| < 0.6$ and $(\sum \vec{p_t})^2 < 0.1$ GeV^2. The detection efficiency is determined by Monte Carlo for each data taking period. It takes into account the track geometrical acceptance ($\simeq 28\%$) and track selection criteria ($\simeq 33\%$), the exclusive proton antiproton identification ($\simeq 45\%$) and the track trigger efficiency ($\simeq 96\%$). The efficiency of higher level triggers ($\simeq 98\%$) is estimated from the data themselves, using prescaled events. The results are summarised in Table 3. The detection efficiency as a function of $m_{\mathrm{p\bar{p}}}$ and $\cos\theta^*$ is presented in Figure 6. The contribution of the different selection cuts is detailed in Table 4.

The dominant source of systematic uncertainty is the selection procedure (10%); other sources are the finite Monte Carlo statistics (5%), the determination of the trigger efficiency (3%) and the background subtraction (1%).

The cross section $\sigma(\gamma\gamma \to \mathrm{p\overline{p}})$ for real photon collisions is extracted as a function of $W_{\gamma\gamma}$ by deconvoluting the two-photon luminosity function and the GDVM form factor [20]. The luminosity functions, as well as the selection and trigger efficiencies, are evaluated for each $W_{\gamma\gamma}$ interval and centre-of-mass energy. An additional uncertainty of 5%, due to the choice of the photon form factor, is included in the systematic uncertainties.

The present $\sigma(\gamma\gamma \to \mathrm{p\overline{p}})$ measurement is compared to the two most recent measurements [4,13] in Figure 7a. The VENUS and CLEO experiments are in agreement inside statistical uncertainties with our results. In Figures 7b, the cross section measurement is compared to the predictions of the three quark model [3] and the recent quark-diquark model calculations [5]. The three quark prediction is based on the leading order QCD calculation of the $\gamma\gamma \to \mathrm{p\overline{p}}$ reaction, using the wave function of Chernyak and Zhitnisky [21]. The diquark prediction is performed with the standard distribution amplitude wave function [5], including first order corrections due to the proton mass. While the shape of the two theoretical curves are quite similar, the normalizations are significantly different. The predictions of the three quark model is about an order of magnitude below the measurement, whereas the quark diquark model reproduce well our data. This discrepancy of the three quark model is most likely due to the inapplicability of the calculation at values of $W_{\gamma\gamma}$ so close to threshold. This result confirms the conclusion of our previous measurement of the reactions $\gamma\gamma \to \Lambda\overline{\Lambda}$ and $\gamma\gamma \to \Sigma^0\overline{\Sigma}^0$ [22].

References

[1] V. M. Budnev *et al.*, Phys. Rep. **15** (1974) 181.

[2] S. J. Brodsky et J. P. Lepage, Phys. Rev. **D 22** (1980) 2157.

[3] G. Farrar, E. Maina and F. Neri, Nucl. Phys. **B 259** (1985) 702; Nucl. Phys. **B 263** (1986) 746.

[4] CLEO, M. Artuso *et al.*, Phys. Rev. **D 50** (1994) 5484.

[5] M. Anselmino, F. Caruso, P. Kroll and W. Schweiger, Int. Mod. Phys. **A 4** (1989) 5213.

[6] C. F. Berger, B. Lechner and W. Schweiger, Fizika **B 8** (1999) 371;
C. F. Berger, *Exclusive Two-Photon Reactions in the Few-GeV Region*, Diploma Thesis, Graz University, 1997;
C. F. Berger and W. Schweiger, private communication.

[7] L3 Collab., B. Adeva *et al.*, Nucl. Instr. Meth. **A 289** (1990) 35;
L3 Collab., O. Adriani *et al.*, Phys. Rep. **236** (1993) 1;
M. Chemarin *et al.*, Nucl. Instr. Meth. **A 349** (1994) 345;
M. Acciarri *et al.*, Nucl. Instr. Meth. **A 351** (1994) 300;
I. C. Brock *et al.*, Nucl. Instr. Meth. **A 381** (1996) 236;
A. Adam *et al.*, Nucl. Instr. Meth. **A 383** (1996) 342.

[8] P. Béné *et al.*, Nucl. Inst. Meth. **A 306** (1991) 150;
D. Haas *et al.*, Nucl. Inst. Meth. **A 420** (1991) 101.

[9] TASSO, M. Althoff *et al.*, Phys. Lett **B 130** (1983) 449.

[10] JADE, W. Bartel *et al.*, DESY 86/043.

[11] TPC/2γ, H. Aihara *et al.*, Phys. Rev. **D 56** (1987) 3506.

[12] ARGUS, H. Albrecht *et al.*, Z. Phys. **C 42** (1989) 543.

[13] VENUS, H. Hamasaki *et al.*, Phys. Lett. **B 407** (1997) 185.

[14] T. Barillari, Cross section measurement of the process $\gamma\gamma \to \mathrm{p\bar{p}}$ in untagged events at $\sqrt{s} = 183$ and 189 Gev with the OPAL Detector at LEP, Photon 2001 Conference.

[15] F. L. Linde, *Charm Production in Two-Photon Collisions*, Ph.D. Thesis, Rijksuniversiteit Leiden, 1988.

[16] F. A. Berends, P. H. Daverfeldt and R. Kleiss, Nucl. Phys. **B 253** (1985) 441.

[17] R. Brun *et al.*, GEANT 3.15 preprint CERN DD/EE/84-1 (Revised 1987).

[18] H. Fesefeldt, RWTH Aachen report PITHA 85/2, 1985.

[19] K. Gzrelak, Exclusive production of charged pion and kaon pairs in photon-photon collisions at LEP, Photon 2001 Conference.

[20] G. A. Schuler, hep-ph/9610406, CERN-TH/96-297.

[21] V. L. Chernyak and I. R. Zhitnitsky, Nucl. Phys. **B 246** (1984) 52.

[22] L3 collaboration, P. Achard *et al.*, Phys. Lett. **B 536** (2002) 24.

	$\sqrt{s}$ (GeV)	$\mathcal{L}$ (pb^{-1})	Events
TASSO (83)	34	74	72
JADE (86)	35 - 44	84	41
TPC/2 (87)	29	75	50
ARGUS (91)	9 - 11	234	60
CLEO (94)	11	1310	484
VENUS (97)	114 - 128	331	311

Table 1: The center-of-mass energy, luminosity and number of events found by each of the previous experiments for the $\gamma\gamma \to \mathrm{p\bar{p}}$ reaction.

Neural Network	Efficiency (%)	Rejection power (%)	Purity (%)	Purity after cuts on the two other NN (%)
e^- NN	89.7	99.4	35.5	64.8
μ^- NN	95.6	99.8	62.9	100.0
h^- NN	53.9	99.4	98.9	99.3

Table 2: The efficiency, rejection power and purity of each neural network for the identification critaria $\zeta > 0.9$, where ζ denotes the output value of the NN. The purity after the cut on the two other NNs is also given.

$\sqrt{s}$ (GeV)	Luminosity (pb^{-1})	Events	Background	Efficiency (%)	$\sigma(\mathrm{e^+e^-} \to \mathrm{e^+e^-p\bar{p}})$ (pb)
183–189	224	220	4.8	3.95 ± 0.06	$24.3 \pm 1.7 \pm 2.8$
192–202	230	203	5.0	3.53 ± 0.06	$24.4 \pm 1.7 \pm 2.8$
205–208	213	181	4.6	3.44 ± 0.06	$24.1 \pm 1.8 \pm 2.8$

Table 3: Integrated luminosity, overall efficiency, number of selected $\mathrm{e^+e^-} \to \mathrm{e^+e^-p\bar{p}}$ events, estimated background and cross section $\sigma(\mathrm{e^+e^-} \to \mathrm{e^+e^-p\bar{p}})$ for each data taking period. The efficiency and cross section refer to the phase-space cuts: $2.1 < m_{\mathrm{p\bar{p}}} < 4.2$ GeV, $|\cos\theta^*| < 0.6$ and $(\sum \vec{p}_t)^2 < 0.1$ GeV^2. The first uncertainty is statistical, the second systematic.

Cut	Efficiency (%)
Two tracks of opposite charge	28
Track selection criteria	33
NN identification	64
Proton identification	88
No photon candidate	88
$(\sum \vec{p}_t)^2$	90
Total	4.1

Table 4: Average efficiency of the different selection cuts used in the analysis for $2.1 < m_{\mathrm{p\bar{p}}} < 4.2$ GeV and $|\cos\theta^*| < 0.6$. The overall efficiency takes also into account the acceptance of the trigger system ($\simeq 94\%$).

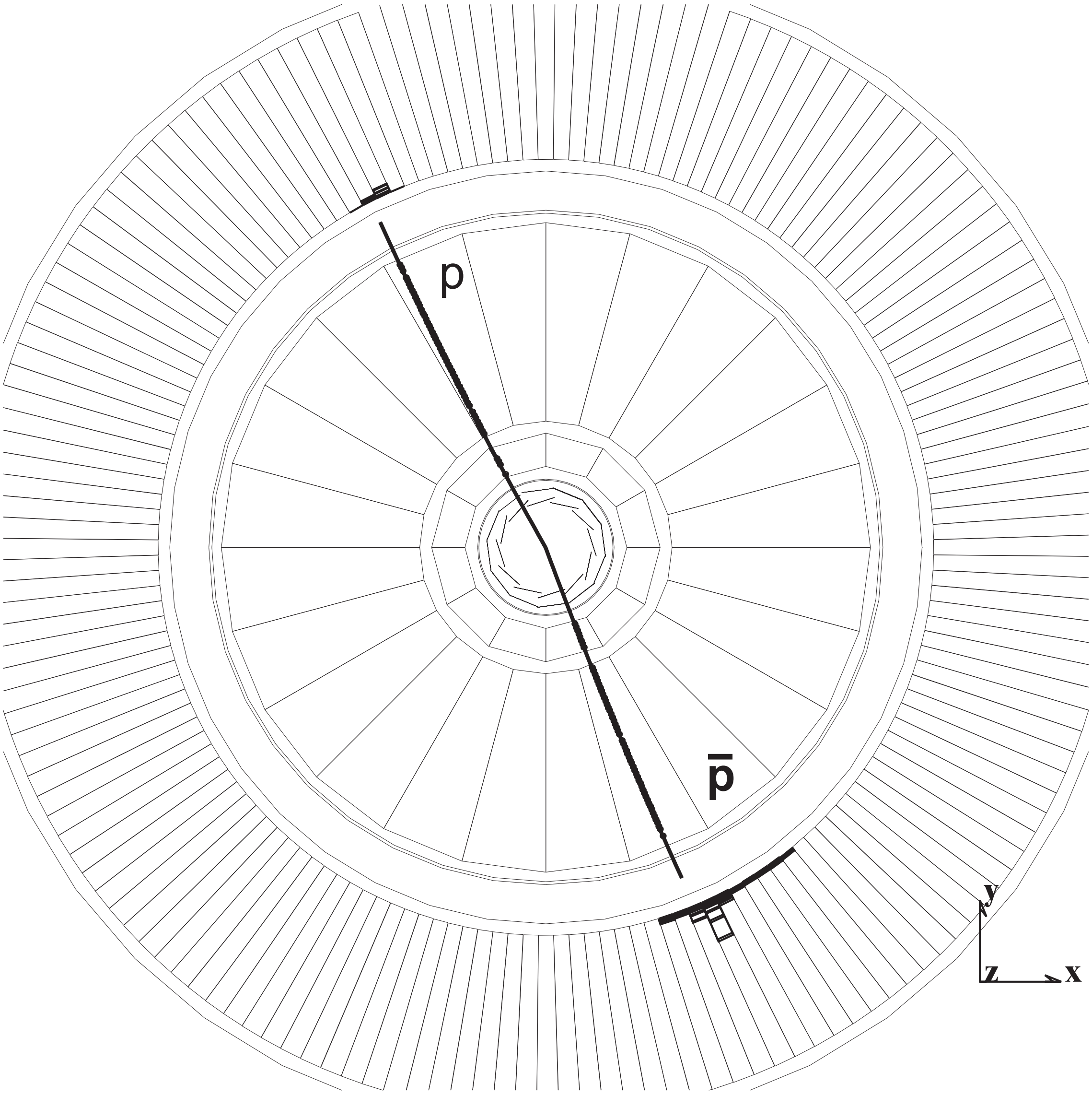

Figure 1: A typical $\gamma\gamma \rightarrow p\overline{p}$ event, displayed in the transverse plane. It illustrates the difference in the electromagnetic calorimeter between the large antiproton signal and the small energy deposit of the proton.

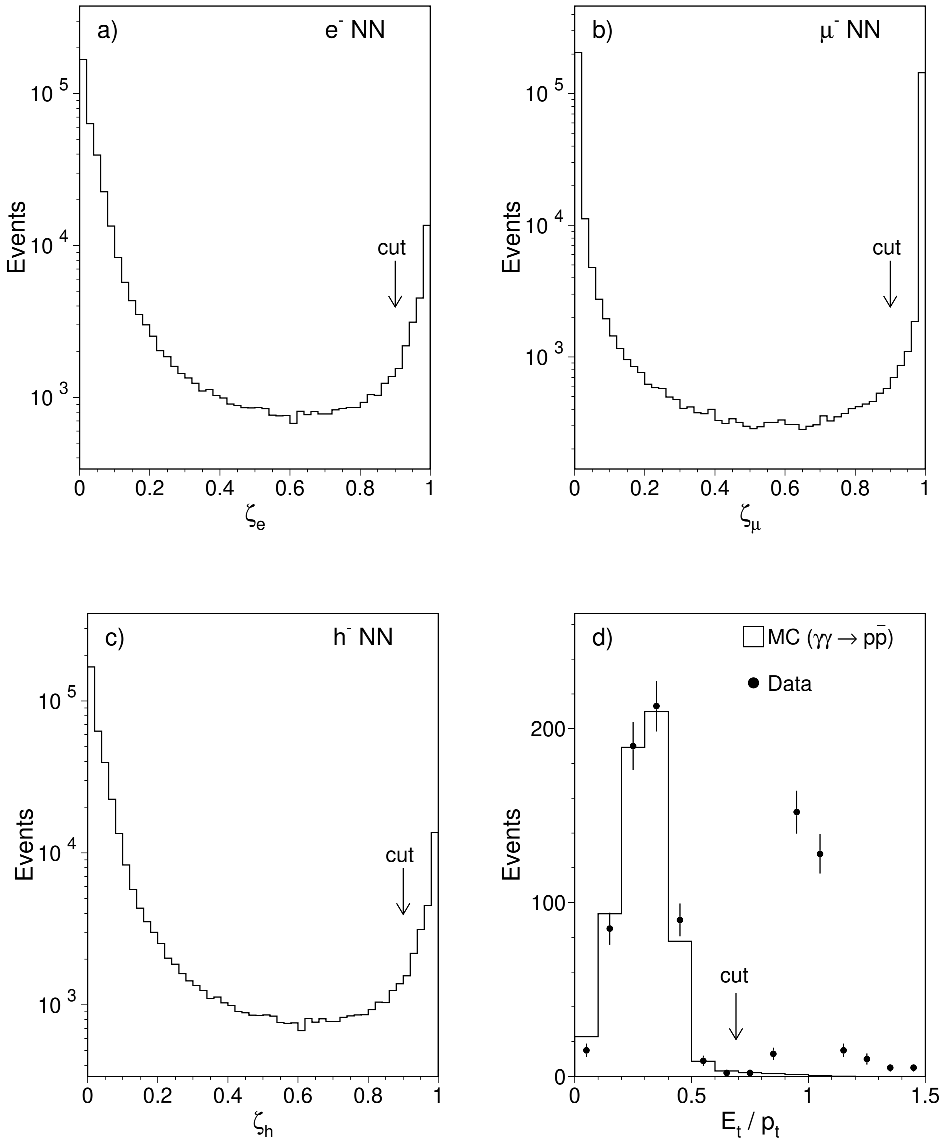

Figure 2: Example of the distributions used for the event selection. a) The output of the e^- NN, b) μ^- NN and c) h^- NN for the data collected at $\sqrt{s}$ = 189 GeV. A particle is identified as an antiproton if the three neural netowrk outputs ζ_e, ζ_μ and ζ_h are greater than 0.9. d) Distribution of the transverse energy deposited in the electromagnetic calorimeter, E_T, and the transverse momentum, p_T, for the exclusive $\gamma\gamma \to p\bar{p}$ Monte Carlo and data. The Monte Carlo is normalized so that the number of data and Monte Carlo events in the region $E_t/p_t < 0.6$ are equal. The right peak not reproduced by the $\gamma\gamma \to p\bar{p}$ Monte Carlo is mainly due to $e^+e^- \to e^+e^-e^+e^-$ events.

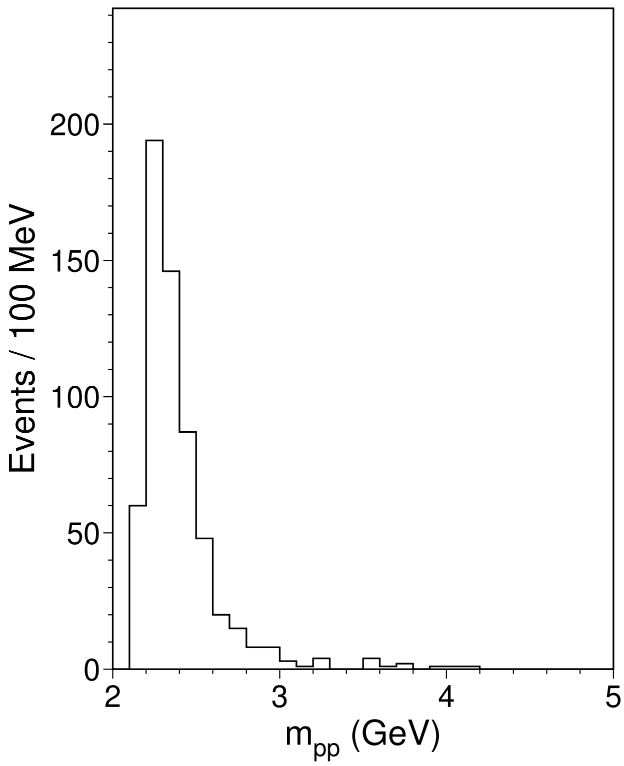

Figure 3: The effective mass of the $p\overline{p}$ pair, $m_{p\overline{p}}$, for the 604 selected events.

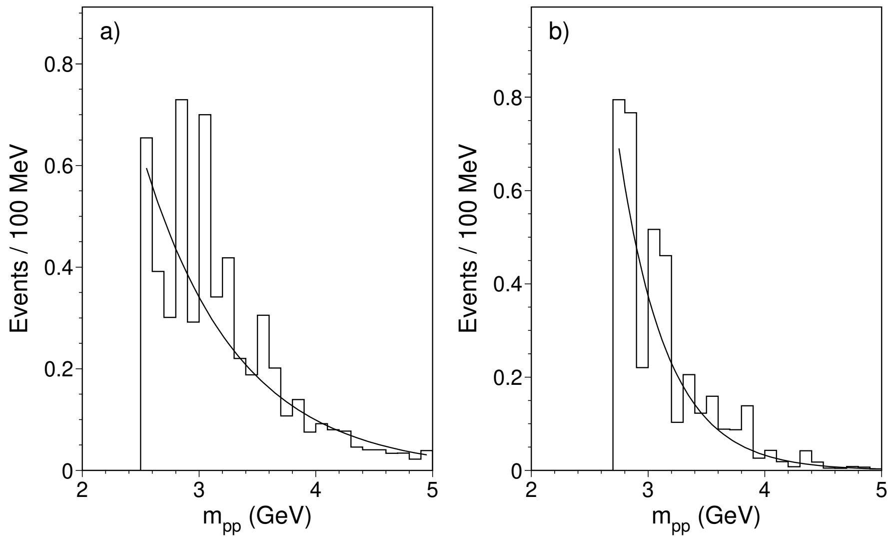

Figure 4: a) The $\gamma\gamma \to K^+K^-$ and b) the $\gamma\gamma \to \pi^+\pi^-$ exclusive background as a function of $m_{p\overline{p}}$. These background are fitted with exponential functions and subtracted bin by bin for cross section determination.

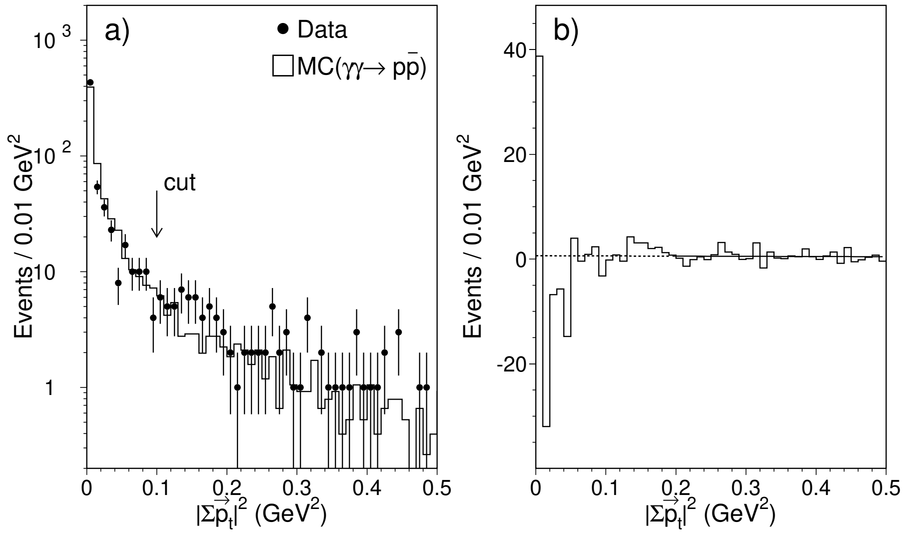

Figure 5: a) The $(\sum \vec{p_t})^2$ distribution of the selected $\mathrm{p\bar{p}}$ sample and the expected distribution from the $\mathrm{e^+e^-} \rightarrow \mathrm{e^+e^-p\bar{p}}$ Monte Carlo. The two distributions are normalized to the first three bins where the inclusive contamination is expected to be negligible. b) The difference between them is fitted with a straight line in the interval 0.2 GeV^2 < $(\sum \vec{p_t})^2$ < 0.5 GeV^2 (plain line). The extrapolation to the region $(\sum \vec{p_t})^2 < 0.1$ GeV^2 (dashed line) gives the inclusive contamination.

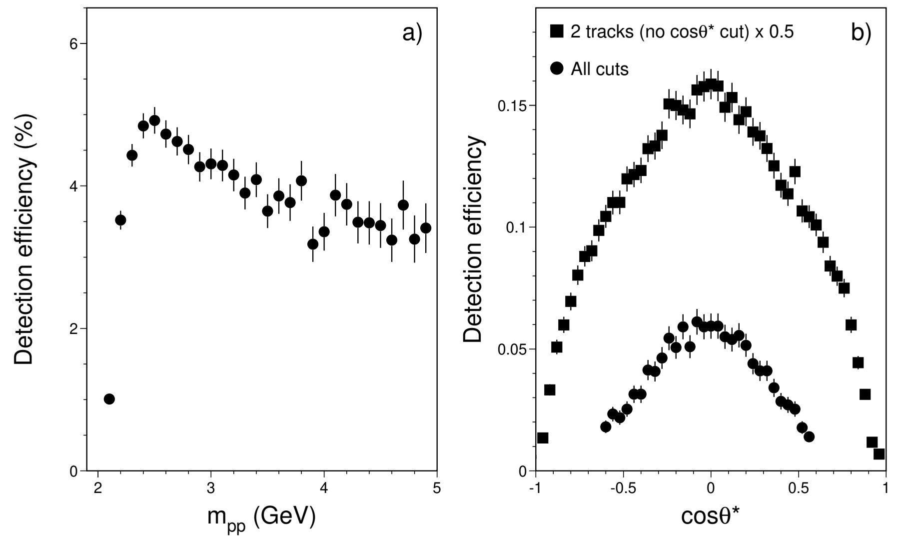

Figure 6: The detection efficiency as a function of a) $m_{\mathrm{p\bar{p}}}$ and b) $\cos\theta^*$ (full circles) for 2.1 GeV $< m_{\mathrm{p\bar{p}}} <$ 4.2 GeV and $|\cos\theta^*| < 0.6$. The two tracks acceptance (no $\cos\theta^*$ cut) is also indicated (full squares). The acceptance is almost limitated to the region $|\cos\theta^*| < 0.6$.

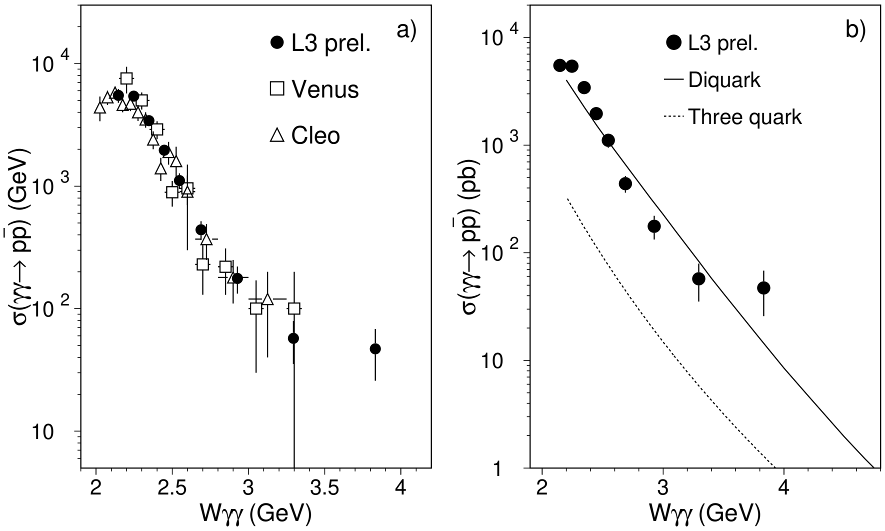

Figure 7: The $\gamma\gamma \rightarrow \mathrm{p\overline{p}}$ cross sections as a function of $W_{\gamma\gamma}$. In a) the results are compared to the one obtained by CLEO [4]. In b) the $\sigma(\gamma\gamma \rightarrow \mathrm{p\overline{p}})$ measurement is compared to the three quark model calculation [3] and to the recent quark-diquark model predictions [5]. Only statistical uncertainties are shown.